Effect of a Chelating Agent on the Physicochemical Properties of TiO$_2$: Characterization and Photocatalytic Activity

Hayat Khan · Dimitrios Berk

Abstract In the current study, it was found that the physiochemical properties of TiO$_2$ are effected with formic acid as a chelating agent in a sol–gel process. From XRD studies it was revealed that due to the chelation of formate group with titanium precursor, anatase/brookite mixture of 86:14 is obtained while the control sample which has been prepared without formic acid showed pure anatase at 400 °C. FTIR studies indicated that, the formate group favored a monodentate mode of coordination with titanium precursor under the effect of addition of increasing amount of formic acid, while under the effect of increasing titanium precursor content the formate group is chelated with titanium atoms in a bidentate bridging mode. In addition, from the FTIR study it was demonstrated that increasing the amount of water in the hydrolysis step, a reduction in the intensity of the carboxylate (COO$^-$) stretches was observed indicating that the titania formate bridging complex becomes weaker, resulting in a weakened titanium gel network structure which could readily collapse during calcination favoring early rutile formation. Raman spectroscopy showed that as a result of sample composite nature and presence of oxygen vacancies as demonstrated by PL analysis causes the broadening and frequency shifting of the Raman bands. Photocatalytic studies demonstrated that the formic acid modified sample composed of anatase/rutile mixture of 94:6 calcined at 600 °C show significantly higher catalytic activity compared to the control sample prepared under similar conditions. Kinetic analysis show first order kinetics for the decomposition of methylene blue, a rate constant (k$_{app}$) of 0.074 min^{-1} was obtained with anatase/rutile (94:6) mixture which is even higher than the Degussa P25 (0.067 min^{-1}).

Keywords Sol–gel synthesis · TiO$_2$ · Calcination temperature · Chelating agent · Photocatalysis

Abbreviations

ART	Anatase to rutile transformation temperature
Δ	Delta represent the difference in asymmetric (v(COO−)as) and symmetric carboxylate (−v(COO−)s)) stretches
C	Reaction concentration
C$_o$	Concentration of organic pollutant
K$_{app}$	Apparent reaction rate constant
CB	Conduction band
VB	Valance band
FWHM	Full width at half maximum
α	Absorption coefficient
E$_u$	Urbach energy
hυ	Photon energy
λ	Wavelength

H. Khan · D. Berk (✉)
Department of Chemical Engineering, McGill University, 3610 University Street, Montreal, QC H3A 2B2, Canada
e-mail: Dimitrios.berk@mcgill.ca

1 Introduction

The photocatalytic application of pure and composite TiO$_2$ depends strongly on crystalline structure, composition, crystallinity, particle size and surface defects; thus there is a need to develop novel routes or improve existing ones for the synthesis of TiO$_2$ with controlled physical and chemical properties to achieve enhanced photocatalytic activity.

Common precursors used to synthesize TiO$_2$ are titanium alkoxides that can be hydrolyzed in the presence of acid catalysts which have an effect on the rate and extent of the hydrolysis reaction, condensation rates, particle morphology, phase transformation and on the structure of the condensed product. Acid catalysts that have been investigated in the past with titanium butoxide as precursor are HCl [1, 2], HNO$_3$ [3, 4], H$_2$SO$_4$, CH$_3$COOH [5] and H$_3$PO$_4$ [6]. Schaefer et al. [7] reported that the purpose of adding acid in the peptization step is to disintegrate the large aggregates into smaller ones by the electrostatic repulsion of charged particles thus decreasing the crystallite size of the formed titania particles. Yu et al. [8] reported that at high acid (HCl) concentration, Ti–OH$_2^+$ groups are formed instead of Ti–OH. Due to charge repulsion between the groups, dehydration hardly occurs, and the TiO6 octahedra prefer to share corners with each other, resulting in TiO$_2$ particles with brookite and rutile structure. Zhang et al. [6] stated that using HNO$_3$ instead of HCl, the obtained TiO$_2$ particles retain the shuttle-like morphology, but smaller particle sizes were obtained than those obtained with HCl. Furthermore, using H$_2$SO$_4$ or H$_3$PO$_4$ results in the formation of spherical amorphous TiO$_2$ at all acid concentrations. The particles obtained with H$_2$SO$_4$ were uniform small spheres having a diameter of about 40 nm; in contrast large sphere particles having diameter of 240 nm were obtained using H$_3$PO$_4$.

In addition to the pH effect, organic acids can act as chelating agents. Nguyen et al. [9] reported that chemical modification of the metal alkoxide by using chelating agents such as acetic acid and acetyl acetone, the final product (TiO$_2$–SiO$_2$) showed high specific surface area. Suresh et al. [10] concluded that an increase in pH causes a decrease in the chelating effect of acetic acid with titanium isopropoxide; as a result a weak gel network structure forms resulting in decreased anatase-to-rutile transformation (ART) temperature. Similarly Yin et al. [11] in their hydrothermal synthesis method explained that chelation of citric acid with TiO6 octahedra and acidification with nitric acid becomes the basis for rutile phase formation due to edge sharing polycondensation between TiO6 octahedra; increase in protonation due to nitric acid further strengthens the chelating phenomenon resulting in enhanced formation of rutile phase.

The role of organic acids to act both as a chelating agent and as an acid catalyst has prompted us to synthesize nano crystalline titanium dioxide from titanium butoxide by the sol–gel method using formic acid (CH$_2$O$_2$), a simple carboxylic acid catalyst. We now report that using formic acid as a chelating agent, a composite mixture of anatase-brookite can be prepared at calcination temperature below 600 °C while anatase–rutile mixture is produced at a temperature above 600 °C. Formic acid modified TiO$_2$ powders have low crystallite size and high Urbach energy value compared to control samples calcined at different temperature. In conclusive approach, the chelating effect of this acid on the characteristics and on the photocatalytic activity of the resulting catalysts has never been explored. Also, not enough literature is available on the effect of calcination temperature on the photoluminescence and Raman properties of TiO$_2$. The objectives of the current paper are:

- To study the effect of chelation on the physicochemical properties (crystalline phase and composition, particle size and crystallinity) of TiO$_2$ using formic acid and to examine the effect of increase in water content (hydrolysis step) on the chelating characteristic of formic acid with titanium precursor to explain the early anatase–rutile transformation phenomenon.
- To study the shift in band gap energy with respect to TiO$_2$ phases and calculated Urbach energy values for the formic acid modified TiO$_2$ powder calcined at different temperatures.
- Photoluminescence properties and Raman spectra of formic acid modified powder calcined at different temperature is investigated to elucidate the variations in these properties (PL and Raman spectra) with the composite nature of the powder.
- Finally the photocatalytic activities of the formic acid modified TiO$_2$ and the control samples prepared without employing formic acid were tested in the photodegradation of methylene blue, methyl orange and mixture of the two.

The binding mode of the formate group to titanium was evaluated by performing an FTIR study. The frequencies of asymmetric ($\nu(COO^-)_{as}$) and symmetric ($\nu(COO^-)_s$) carboxylate vibrations were determined in FTIR spectra, and this difference, ($\Delta = \nu(COO^-)_{as} - \nu(COO^-)_s$) was used as a basis to find the carboxylate binding; the activities of the prepared catalysts were evaluated by comparison with the commercially available Degussa P25 to establish the hypothesis for enhanced activity.

2 Experimental Materials and Methods

2.1 Catalyst Preparation

The nanoparticles of TiO$_2$ were prepared by the sol–gel method. Titanium butoxide (Ti(OBu)$_4$, purum ≥97.0 % gravimetric), formic acid (CH$_2$O$_2$, ~98 %, Fluka) were supplied by Sigma Aldrich. Anhydrous ethyl alcohol (C$_2$H$_6$O) was supplied by Commercial Alcohols (Boucherville, Quebec, Canada). All the chemicals were used as received without any further purification. Reverse osmosis water was used throughout this research.

The titanium precursor, titanium butoxide (5 ml) was dissolved in anhydrous ethyl alcohol (10 ml) followed by the addition of formic acid (2.2 ml) and water (5 ml) under strong magnetic stirring. The resulting solution was stirred for 2 h, hydrolysis and polymerization reactions occurred in the mixture which resulted into a milky sol of hydrated titanium hydroxide. The sol solution was aged for gelation for 6 h at ambient temperature followed by drying in oven at 85 °C for 24 h. The dried powder or gel (pulverized to powder) was subsequently calcined at the desired temperature (400, 500, 600 and 700 °C) for 1 h in air at a heating rate of 10 °C per min to form crystalline TiO_2 nanoparticles. The molar ratios were varied throughout the experiment. To investigate the influence of formic acid, the formic acid/titanium butoxide/ethyl alcohol/water molar ratio was varied by keeping constant the titanium butoxide/ethyl alcohol/water ratio at X:1:3:5 while the formic acid content (X) changed from 0, 1, 2 and 3. These samples were labeled as TFA_0, TFA_1, TFA_2 and TFA_3, respectively. To investigate the influence of water on acid chelation, titanium butoxide/ethyl alcohol/formic acid molar ratio was kept constant at 1:3:1 while the water content varied from 5, 10 and 15, these samples were designated by TW_5, TW_{10} and TW_{15}. Also to study the effect of titanium butoxide on acid chelation, ethyl alcohol/formic acid/water molar ratio remained constant at 3:1:5 while the titanium butoxide content is varied from 1, 2 and 3, these samples were identified by TTB_1, TTB_2 and TTB_3, respectively.

2.2 Catalyst Characterization

The crystal structure of the prepared catalysts was examined on a Phillips PW 1710 diffractometer using monochromatic high intensity Cu Kα radiations ($\lambda = 0.15418$ nm). The crystallite size was calculated by taking into account the most intense reflections (101) anatase, (121) brookite and (110) rutile phase using the Debye–Scherrer formula. The phase composition of the composite powders were estimated by using the Zhang and Banfield equations [12]. To evaluate the carboxylate binding mode and the presence of different bonding vibrational frequencies, infrared spectra was recorded on a Bruker Tensor 27 FTIR with OPUS data collection program (V 1.1), in the energy range of 4,000–400 cm^{-1}. The pre-calcined powder was mixed with the reference potassium bromide (KBr). The band gaps of the catalyst samples were calculated by using the Kubelka–Munk function. The absorption spectrum of the catalyst using KBr as a reference was measured on a thermo scientific UV–Vis Evolution 300 spectrophotometer which is equipped with integrated Pike technologies EasiDiff, diffuse reflectance accessory in the range 190–800 nm range. High resolution transmission electron microscope images of the synthesized samples were obtained with Phillips CM200

TEM operated at 200 kV. Photoluminescence (PL) spectra obtained at an excitation wavelength of 320 nm of Xe lamp were recorded on FluroMax-2 spectrofluorometer and Raman spectra were recorded at room temperature using a Thermo Fisher Scientific DXR dispersive Raman spectrometer under solid LED 532 nm laser excitation.

The photocatalytic activity of the prepared TiO_2 catalysts was investigated for the degradation of methylene blue (MB) and methyl orange (MO) solutions. The cylindrical reactor contained 2.4 L aqueous solution of 6.0 mg L^{-1} of the dye and 0.1 g L^{-1} of the prepared TiO_2 powder. A single UV light source (max. output at 254 nm, Germicidal UVC lamp, Atlantic Ultraviolet Corp. GPH212T5L/4) protected in a quartz sleeve was placed vertically at the center point inside the reactor. The reactor solution under constant magnetic stirring was bubbled continuously with external air throughout the experiment. UV illumination was supplied for 1 h experimental duration. A sample of 5 ml was withdrawn at regular interval, before analysis the sample suspension was filtered to remove the photocatalyst particles. The photocatalytic degradation of MO and MB was followed by UV–Vis spectrophotometer by measuring at 466 and 664 nm, respectively, the maximum absorbance of the solution fetched every 10 min.

3 Result and Discussion

3.1 TiO₂ Phase Formation, Transformation and Crystallite Size

To evaluate the formation of TiO_2 phases in the final product by employing formic acid as an acid catalyst, the synthesized powders (TFA_1) were calcined at different temperatures. Figure 1 shows the X-ray diffraction patterns of the synthesized TiO_2 powders calcined at 400, 500 and 550 °C. The patterns show that at 400 and 500 °C the powders were composite mixtures of anatase and brookite (minor phase) while pure anatase formed at 550 °C. At 600 °C rutile (minor phase) was obtained with the main anatase phase, and at 700 °C rutile was the dominant phase in the calcined powder (see Fig. 1 inset). This suggests that upon heating, the phase transition among the TiO_2 crystalline phases follows the sequence of brookite to anatase to rutile.

$$TiO_2(brookite) \rightarrow TiO_2(anatase) \rightarrow TiO_2(rutile)$$
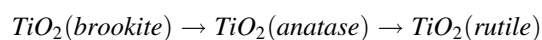
The series of powders prepared in the absence of formic acid (TFA_0) and calcined at 400, 500 and 600 °C (see Table 1) result in the formation of anatase TiO_2 while a further increase in temperature initiates the transition of anatase to rutile. This implies that formic acid plays a significant role in crystalline phase formation. Brookite as a minor phase was observed in the samples synthesized in the presence of formic acid, but its

Fig. 1 X-ray diffraction patterns of sample powder (TFA$_1$) calcined at 400, 500, 550, (*inset*) 600 and 700 °C
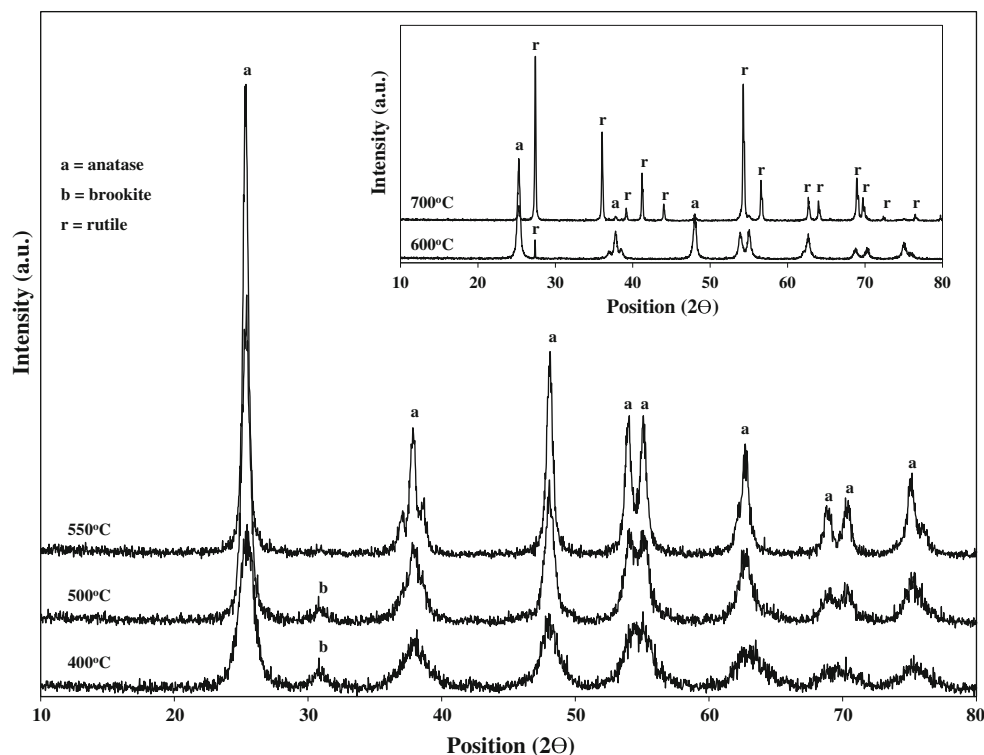
proportion decreases as shown in Tables 1 and 2 with an increase in the molar ratio of formic acid or decrease in the pH value of the solution (mole ratio of formic acid used, 1 (pH 3.5), 2 (pH 2.3) and 3 (pH 1.8), respectively). Increase in the amount of formic acid during the hydrolysis of titanium butoxide, enhances the proportion of protons [H$^+$] which results in the formation of Ti–OH$_2^+$ ions in the reacting solution instead of Ti–OH. It may be possible that during the polycondensation process, the Ti–OH$_2^+$ species result in greater dehydration. As a consequence the resulting TiO6 octahedra may share corners with other octahedra thus resulting in the formation of anatase (see Fig. 2, schematic I in supplementary material). On the other hand, at the low concentration of [H$^+$], incomplete dehydration of Ti–OH group may occur during the polycondensation process, which means that the TiO6 octahedra will share edges and corners and result in the formation of brookite phase (see Fig. 2, schematic II in supplementary material). Therefore, low molar ratio of formic acid will hinder the rearrangement of TiO6 octahedron units into the pure anatase phase; as a consequence the formation of the minor brookite phase occurs. In contrast, in the absence of formic acid during the hydrolysis step, only the addition of water and an increase in its amount will accelerate the rearrangement of TiO6 octahedra units; thus the rate of crystallization and nucleation increases which favors the formation of pure anatase phase [13].

In order to test if the above results were due to chelation effect of formic acid and not the pH value, TiO$_2$ powders

Table 1 Effect of calcination temperature on TiO$_2$ crystallite size and weight fractional composition (the numbers in parentheses) in the presence (TFA$_1$, molar ratio of formic acid used = 1) and absence of formic acid (TFA$_0$)

Catalyst powder	Calcination temperature (°C)	Anatase crystallite size (nm)	Brookite crystallite size (nm)	Rutile crystallite size (nm)
TFA$_1$	400	6.9 (0.86)	5.8 (0.14)	
	500	11.5 (0.93)	4.6 (0.06)	
	550	22.9 (1.0)		
	600	26.6 (0.94)		23.1 (0.06)
	700	55.2 (0.07)		55.4 (0.93)
TFA$_0$	400	8.6 (1.0)		
	500	17.2 (1.0)		
	600	19.8 (1.0)		
	700	23.0 (0.26)		34.6 (0.74)

were prepared at the same pH values (3.5, 2.3 and 1.8) as before by the addition of nitric acid but in the absence of formic acid. The XRD spectra (see S1 in Supplementary Information) show that these catalysts were composed only of anatase phase indicating that in the synthesis process using formic acid, it is the pH dependent chelation property that plays a significant role in composite phase formation. These results are in contrast to those recently obtained by Liu et al. [14] who showed that the phase transition from H-titanate to anatase, brookite and rutile depends on the acid (HNO$_3$) concentration; however it should be pointed

Table 2 Effect of formic acid (TFA$_x$, where molar ratio x = 2 and 3) and water (TW$_x$, where molar ratio x = 10 and 15) on TiO$_2$ crystallite size and weight fractional composition (the numbers in parentheses), catalyst powders were calcined at 400 and 600 °C

Catalyst powder	Calcination temperature (°C)	Anatase crystallite size (nm)	Brookite crystallite size (nm)	Rutile crystallite size (nm)
TFA$_2$	400	7.7 (0.91)	5.6 (0.09)	
TFA$_3$		6.8 (0.97)	5.1 (0.03)	
TFA$_2$	600	24.3 (1.0)		
TFA$_3$		21.8 (1.0)		
TW$_{10}$		30.6 (0.87)		69.2 (0.13)
TW$_{15}$		34.5 (0.87)		69.2 (0.22)

out that Liu et al. used the hydrothermal process and a different precursor from those used in the present work.

The effects of the concentration of formic acid and water on ART temperature are illustrated in Tables 1 and 2. The prepared powders were calcined at 600 °C because at this temperature rutile phase formation occurs in the TFA$_1$ catalyst sample (see Table 1). The factor which determines the formation of rutile and its proportion in the final powder is the amount of water added during the catalyst synthesis process. Increase in molar ratio of formic acid in the powders TFA$_2$ and TFA$_3$ causes an improved chelation that results in the formation of pure anatase phase (see Table 2). From this result it is clear that an increase in the amount of formic acid has a positive increasing effect on ART. The increase in formic acid increases the acidity of the sol; as a consequence it increases the chelating effect of the formate group. This increase in chelation results in a strong gel network and consequently delays the formation of rutile

phase at 600 °C as observed in TFA$_1$ powder. The XRD patterns of the catalyst powder prepared under the influence of an increase in the amount of water in the catalyst synthesis process shows the growth of rutile peaks (see Fig. S2 in Supplementary Information). Increasing the amount of water during the hydrolysis step leads to enhanced formation of rutile phase. Increasing the water-to-precursor ratio accelerates the hydrolysis and crystallization reactions; primary particles aggregate to form larger secondary particles that are thermodynamically disposed to transform to rutile; illustrate the fact that anatase to rutile transition temperature decreases as the water content increases.

Investigating the influence of water and formic acid on TiO$_2$ crystallite size, we observed that increasing the amount of water during the hydrolysis step results in the increase of TiO$_2$ crystallite size as shown in Table 2 whereas increasing the molar ratio of formic acid causes a decrease in TiO$_2$ crystallite size as presented in Tables 1 and 2. Increasing the amount of water causes the enhanced hydrolysis of alkoxide precursor; as a consequence a significant amount of Ti–OH network groups which are beneficial for the formation of TiO6 octahedra units are produced. The variation in crystallite size due to the increase in molar ratio of water can be ascribed to the freedom of TiO6 units arrangement. When the water content is higher, the space is larger for the TiO6 octahedra units to adjust themselves [13]. Thus, the rearrangement of these units will be more regular and will result in the formation of a structure with large network; therefore the TiO$_2$ crystallite size increases with increase in the amount of water. In contrast an increase in the amount of formic acid results in low crystallite size of TiO$_2$ particles; acid causes a decrease in the pH of the sol. As a consequence

Fig. 2 Proposed schematics of anatase and brookite formation from chelated TiO6 octahedra
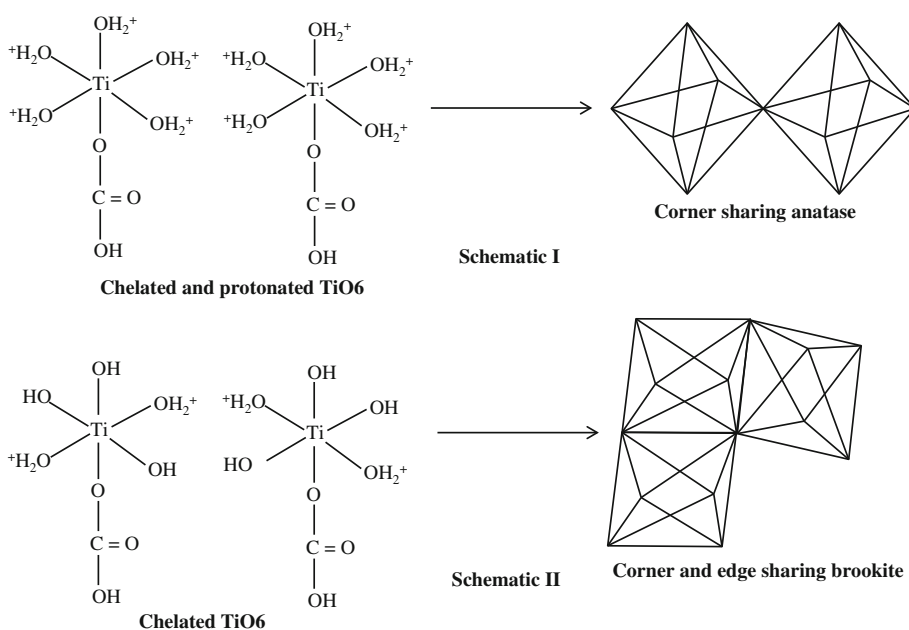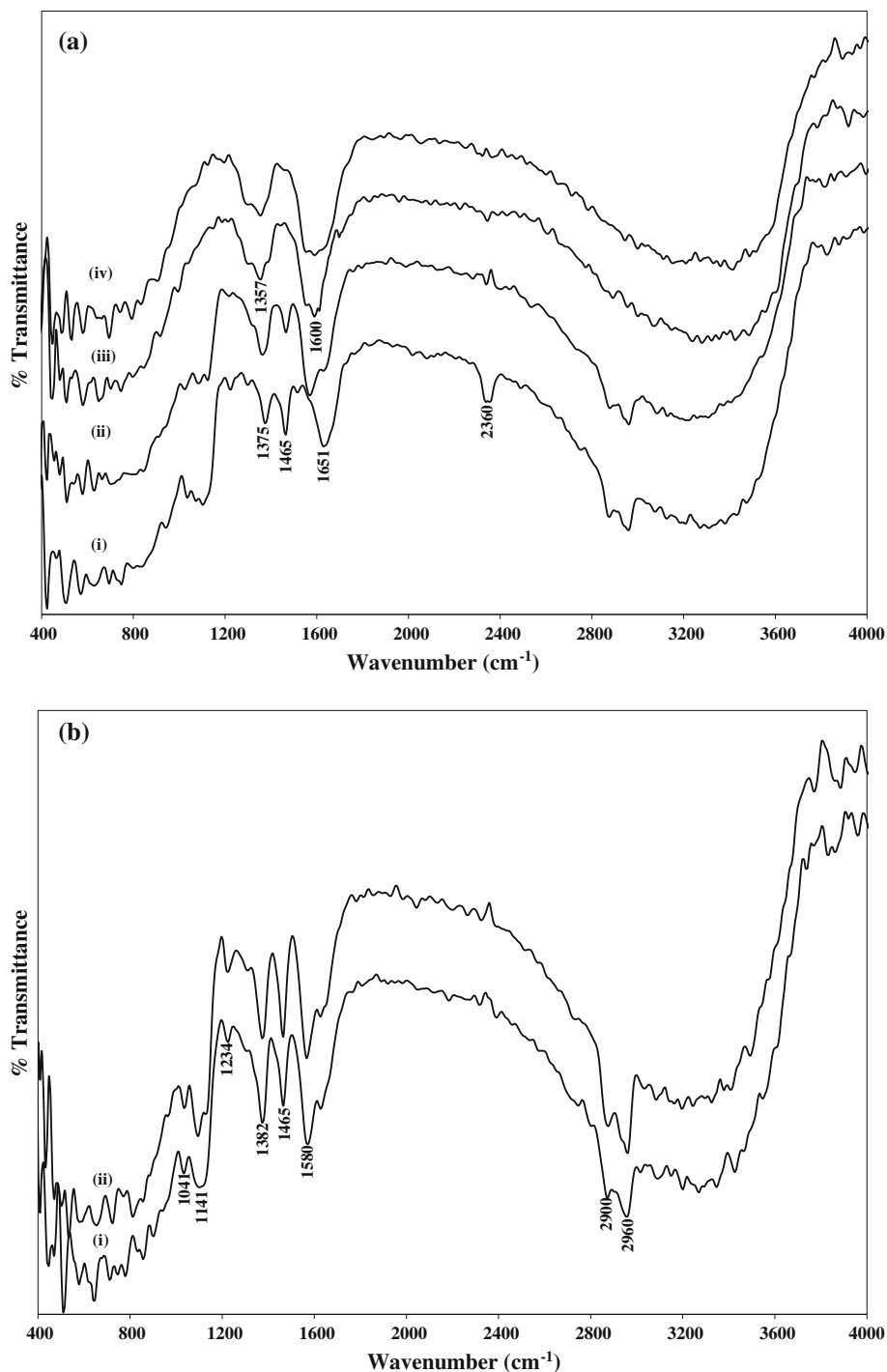
Fig. 3 FTIR spectra of TiO$_2$ powder; **a** Influence of formic acid—(i) TFA$_0$ (ii) TFA$_1$, (iii) TFA$_2$, and (iv) TFA$_3$; **b** Effect of titanium butoxide—(i) TTB$_2$ and (ii) TTB$_3$

dissolution of TiO$_2$ particles followed by slow recrystallization of titania particles occurs [15], leading to a decrease in crystallite size.

3.2 FTIR Spectroscopy Analysis

Figure 3a, b depicts the FTIR spectra of the powder prepared under the influence of an increase in the molar ratio of formic acid and titanium butoxide, respectively. Figure 3a (spectrum (i)) shows the spectrum of the sample prepared without employing formic acid (control sample, TFA$_0$). The broad absorption peak in the range of 2,800–3,600 cm^{-1} is due to OH stretching modes from molecular water; the intensity of this peak is lowered on adding an increasing amount of formic acid, spectra (ii–iv). Several peaks in all spectra in the range of 400–1,000 cm^{-1} are attributed to oxygen vibration, Ti–O–Ti vibrational frequencies and Ti–O stretches. Peaks at 1,375 and 1,465 cm^{-1} stands for the δ_s

and δ_{as} (CH$_3$)-group of titanium butoxide adsorbed on the surface of TiO$_2$. The δ_s-CH$_3$ peak shifted to lower wavenumber of 1,357 cm^{-1}, which is attributed to $\nu(COO^-)_s$ symmetric carboxylate stretch and δ_{as}(CH$_3$) peak diminishes with the addition of formic acid. The peak at 2,360 cm^{-1} is unexpected and assigned to atmospheric carbon dioxide adsorption. The peak at 1,651 cm^{-1} is attributed to physically adsorbed water molecules (δ_{H-O-H}), this peak is shifted towards lower wavenumber of 1,600 cm^{-1} in presence of formic acid and is attributed to $\nu(COO^-)_{as}$ asymmetric carboxylate stretch.

Formic acid belongs to carboxylic acid family, which not only acts as an acid catalyst, but also acts as a ligand by forming different binding complexes. The carboxylate group has versatile coordination behaviour and for this reason it can be binded with another metal atom through ionic, monodentate, bidentate chelating and/or bidentate bridging modes. To determine the mode of carboxylate group binding to the metal atom, the difference between the frequencies of asymmetric and symmetric carboxylate stretches is calculated ($\Delta = \nu(COO^-)_{as} - \nu(COO^-)_s$) [16]. In Fig. 3a, for the spectra (ii–iv), Δ is calculated to be 243 cm^{-1}; this value is much higher than that of $\Delta_{sodium\ benzoate}$ (139 cm^{-1}), thus proving that the formate group is bound to titanium atoms through monodentate coordination (see Fig. S3—schematic I in Supplementary Information). To investigate the effect of water on the monodentate network structure, the amount of water is increased in the hydrolysis step i.e. using mole ratio 10 and 15 respectively in the catalyst samples containing 1.0 mol ratio of formic acid. The figure (not shown here) illustrates that the peaks corresponds to monodentate formate group, $\nu(COO^-)_s$ and $\nu(COO^-)_{as}$ become weaker in intensity compared to OH peak at 2,800–3,600 cm^{-1}. The increase in the amount of water alters the pH of the solution (mole ratio of water used, 10 (pH 4.5), 15 (pH 5.8)) as well enhances the hydrolysis reaction and weakens the polymeric structure of the gel. This means that chelation of the carboxylate group is weakened as evident from the reduced intensity of the COO$^-$ stretches, facilitating increased hydrolysis and condensation rate and causing a reduction in ART temperature which increases the fraction of rutile phase in the final powder (see Table 2). This result illustrates that FTIR results are in agreement with the XRD studies.

Figure 3b shows the FTIR spectra of the powders prepared under the influence of increasing titanium butoxide amount. The spectra show asymmetric (1,580 cm^{-1}) and symmetric (1,382 cm^{-1}) carboxylate stretches. In addition, the peaks observed at 1,234, 1,103 and 1,041 cm^{-1} may corresponds to ν(C–O–C) and O–CH$_3$ group or to δ(CCH)+δ(CH$_3$, CH$_2$) respectively. Moreover, peaks at 2,900 and 2,960 cm^{-1} are assigned to asymmetric stretching vibration of CH$_3$ group. The calculated experimental value for the carboxylate

stretches, $\Delta = 198$ cm^{-1}, is consistent with the literature value for ionic formate (HCOO$^-$) $= 201$ cm^{-1} [17]. According to the guideline reported elsewhere [18], for carboxylate group to exists in bidentate bridging, the $\Delta(COO-)_{carboxylate\ complex} \leq \Delta(COO-)_{sodium\ salt}$. Therefore, the Δ value of 198 cm^{-1} indicates that the formate group binds to a titanium center in a bidentate bridging mode under the effect of increasing titanium butoxide (see Fig. S3—schematic II in Supplementary Information). Due to the chelating nature of the formate group, it will not be easy to dehydrate the powder upon calcination. Therefore anatase phase is maintained at 600 °C without starting the transformation into rutile phase as occurred in the TTB$_1$ powder (not shown here).

3.3 Bang Gap Energies Analysis

The band gap value of the TiO$_2$ catalysts were calculated using diffuse reflectance spectra in conjunction with modified Kubelka–Munk (K–M) function. The bang gap values of TFA$_1$ and TFA$_0$ samples calcined at different temperature are given in Table 3; for some of the selected TiO$_2$ samples K–M plot (($\alpha h\upsilon)^{1/2}$ is plotted versus photon energy, hυ (eV)) are shown in Fig. 4. The optical band gap was determined by extrapolating the linear portion of the spectra until it intersect hυ axis (x-axis) at E$_g$. The band gap value (ΔE_g) for TiO$_2$ crystallite forms are: anatase (3.21 eV), brookite (3.13 eV) and rutile (3.0 eV) [19]. Literature shows small variations in the band gap value of TiO$_2$ polymorphs and this difference is being attributed to crystalline size, the impurities content, variation in the reaction stoichiometry of the synthesis technique and the type of electronic transitions [20]. In addition, it may also be true that variation in absorption spectra is dependent on the formation of composite mixture of two or three crystalline form of titania, which are, anatase-brookite, anatase–rutile and anatase-brookite-rutile. It is obvious that a sample containing high percentage of anatase or brookite the absorption onset moves towards shorter wavelengths; in contrast, increase in rutile percentage will shift the absorption spectrum towards longer wavelength. Hence in broad spectrum, pure TiO$_2$ band gap energy is a function of particle size and for composite sample it is a function of particle size and phase composition and surface reconstruction during calcination.

As shown in Fig. 4 the shifting of K–M spectra towards longer wavelength is less for the anatase-brookite in comparison to a composite mixture of anatase–rutile; this may be due to the very stable nature of rutile phase. Both anatase and brookite are metastable, and due to reversible random phase transitions, the shift in absorption spectra for longer wavelength is minimum. Also, the intensity of the K–M spectra for anatase-brookite composite was higher than anatase–rutile composite, because of multiple scattering, which implies the

Table 3 Band gap and Urbach energy (E$_u$) values of the TiO$_2$ powder synthesized in the presence of formic acid (TFA$_1$, molar ratio of formic acid used = 1) and in absence of formic acid (TFA$_0$) and calcined at different temperature

Catalyst powder	Calcination temperature (°C)	Band gap (eV)	Urbach energy (meV) (correction factor)
TFA$_1$	400	3.13	336.9 (r^2 = 0.9885)
	500	3.06	136.1 (r^2 = 0.9891)
	550	3.01	134.1 (r^2 = 0.9993)
	600	2.94	129.2 (r^2 = 0.9969)
	700	2.81	45.6 (r^2 = 0.9887)
TFA$_0$	400	3.0	119.7 (r^2 = 0.9864)
	500	2.97	116.4 (r^2 = 0.9804)
	600	2.93	91.1 (r^2 = 0.9868)
	700	2.81	43.7 (r^2 = 0.9806)

presence of large number of particles with decreased particle size. It was observed that as the particle size increases both a decrease in the reflectance intensity value and in the straight portion (absorption tail) of the K–M spectra occur. The absorption tail is also known as Urbach tail and the energy associated with this tail is known as Urbach energy [21] and is given by $\alpha = \alpha_o \exp((h\upsilon - E_o)/E_u))$, where α is the absorption coefficient, α_o and E_o are material properties, $h\upsilon$ is photon energy and E_u is the Urbach energy. Urbach energy values are calculated by plotting $\ln\alpha$ versus E ($h\upsilon$) (see Fig.

S4 in Supplementary Information), the reciprocal of the slope of the linear portion, gives the value of E_u. The Urbach energy values are given in Table 3, the broadness of the Urbach tail is the consequence of structural disorder such as crystalline disorder due to large amount of hydroxyl groups, oxygen defects, thermal disorder contributed by lattice phonons-electron interaction and different grain boundary defects [21]. The Urbach energy values are high for pure anatase and composite mixture (anatase-brookite) calcined at lower temperature due to greater crystal disorder (may be somewhat amorphous nature and impurities), metastability and lower crystallinity. These defects are getting minimized with lowering of Urbach energy on the consequence of increase in calcination temperature and in effect crystallite phase transformation, decrease in crystal deformation through increase in crystallinity with more order structure, stability and particle size occurs. In general as shown in Table 3 the formic acid modified samples (TFA$_1$) have higher Urbach energy value compared to TFA$_0$, this may be due to the chelating nature of the formic acid that resulted in composite mixture of anatase-brookite at 400–500 °C and anatase–rutile at 600 °C, respectively.

3.4 Transmission Electron Microscope Analysis

The bright filed TEM images of sample (TFA$_1$) powder calcined at 400, 600 and 700 °C are shown in Fig. 5a–c.
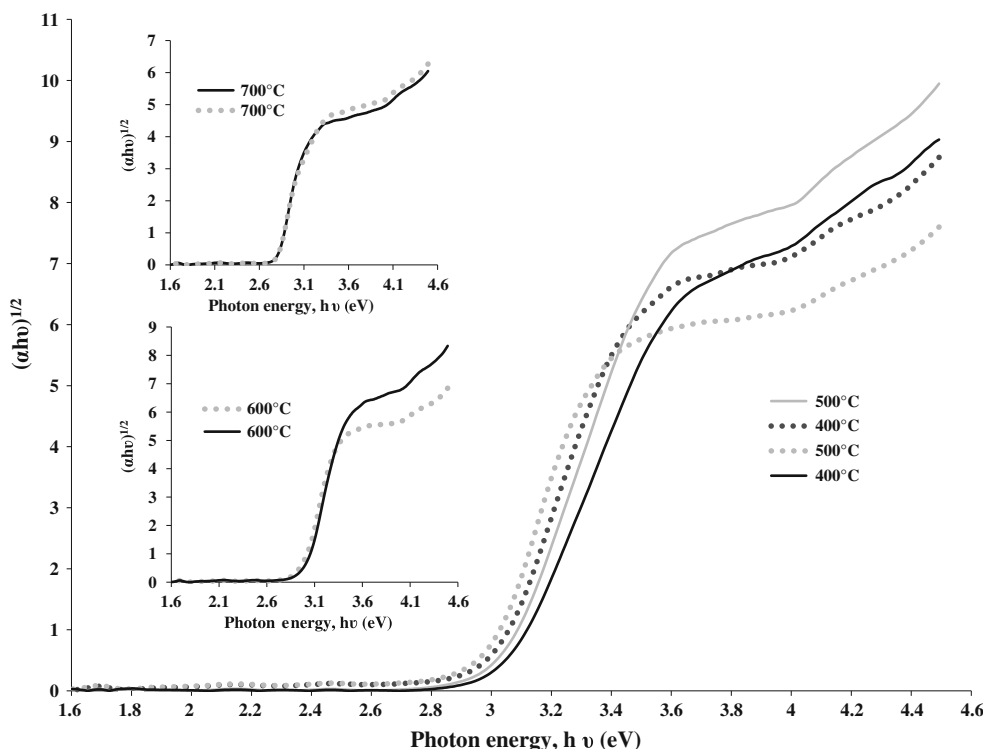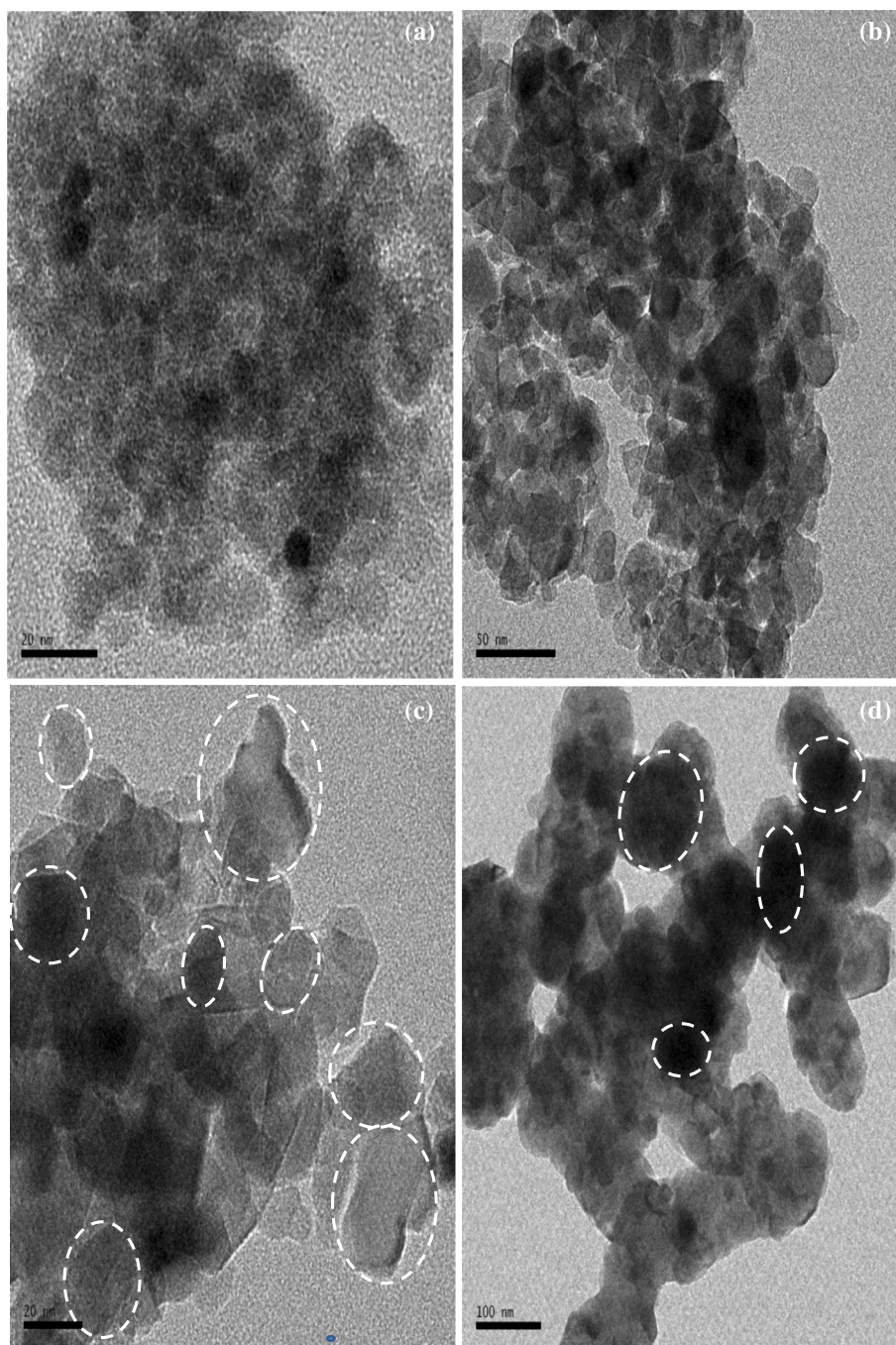

Fig. 4 Kubelka–Munk (K–M) plots; *full lines*—TFA$_1$ and *dotted lines*—TFA$_0$ powder calcined at different temperatures

Fig. 5 TEM images of the synthesized samples, **a** TFA$_1$ calcined at 400, **b** 600, **c** and 700 °C; **d** TFA$_0$ calcined at 700 °C

An increase in temperature does not only result in the increase of particle size but also decreases the amorphous content; as a consequence the particles are more distinct and crystalline in nature.

The HRTEM image of the sample (TFA$_0$) calcined at 700 °C is presented in Fig. 5d, the figure shows that the packing of the structural units are irregular, the particles seem to be encapsulated indicating a cloudy aspect and visually it is difficult to differentiate particles from each other. Such morphology may be due to the absence of

formic acid because protons from the acid medium limit the condensation and allow gelation, favor the formation of more uniform and distinct crystalline particle morphology. Moreover, XRD analysis shows that the sample is a composite mixture containing 75 % rutile, the particle size of rutile is small in comparison to TFA$_1$ powder (see Fig. 5c) containing 93 % rutile. Some of the rutile particles are highlighted with dashed circles. The well-defined circles in the SAED patterns (see Fig. S5 in Supplementary Information) further clarify that the powder has a well defined

crystalline morphology, the SAED results support the XRD results (see Fig. 1).

3.5 Photoluminescence Analysis

PL analysis is a tool in providing useful information on electronic and optical properties of TiO$_2$ materials. Little is known about the PL properties of TiO$_2$ calcined at different temperatures; therefore we attempt to explain the PL spectra features of TFA$_1$ (shown in Fig. 6) and TFA$_0$ (not shown here) powders prepared at 400–700 °C. On comparing the two PL spectra no observable change in peak positioning or the appearance of any new PL peak was recorded except variation in peak intensity and an overall decrease in PL intensity was observed for TFA$_1$ powder which is prepared by employing formic acid. PL emission is the result of electron–hole recombination, thus the decrease in PL intensity of TFA$_1$ powders is attributed to the catalyst composite nature (anatase-brookite at 400 and 500 °C and anatase–rutile at 600 and 700 °C) compared to TFA$_0$ powders composed of pure anatase. The anatase-brookite or anatase–rutile heterojunctions enhance charge separation and prevent the recombination of photogenerated charge carriers. The PL intensity of the synthesized powders (TFA$_1$) was noted to decrease with the increase in calcination temperature; our results contradict the trends observed by Mathpal et al. [22]. In the TFA$_1$ PL spectra excited with 320 nm, the UV emission peak at 394 nm is attributed to the phonon assisted indirect transmission from the center of Brillouin zone to the edge, Γ_3 to X_{1b} (where Γ denotes the center of Brillouin zone (BZ) and X denote the edge) while the one at 418 nm is ascribed to the phonon assisted indirect transition but from the edge to the center of the Brillouin zone (X_{1a} to Γ_{1b}) [23]. The intensity of both these peaks, 394 and 418 nm (denoted by dotted line) are weakened in the TiO$_2$ powder calcined at 600 and 700 °C, this may be due to the presence of rutile phase. The sample calcined at 700 °C is composed of anatase–rutile (1:99), the powder showed absorption spectrum in the visible region (see Table 3) as a consequence the UV peak at 394 nm is completely diminished. Also, the lower band gap of the rutile nanocrystals creates energy wells that trap electrons [24], as a result the radiatively back transferring of photogenerated electrons from the conduction band to the valance band is minimized. The minor emission peak at 411 nm probably originates from the radiative defects related to oxygen vacancies. The peak at 436 nm is attributed to self-trapped excitons localized on TiO6 octahedra and the emission peaks at 449 and 456 nm are related to surface states (Ti–OH) [25]. Oxygen vacancies with two or one trapped electrons (F color center or F$^+$ color center) are assigned to the peak at 461 nm, whereas, oxygen vacancies with two trapped electrons are

represented by the peak at 465 nm [26, 27]. The emission peak at 471 nm may be due to band edge emission or related to crystal defects such as oxygen vacancies or interstitial sites in TiO$_2$. Ti^{+4} ions adjacent to oxygen vacancies (intra gap surface states) or charge transfer from Ti^{+3} to oxygen anion in a TiO6 complex associated with oxygen vacancies at the surface is attributed to the peak at 490 nm. The formation of oxygen defect states (TiO$_{2-x}$) located near the bottom of the conduction band is assigned to the peak at 490 nm [28]. A broad emission in the range from 500 to 550 nm is assigned to the surface states (Ti^{+4}–OH) and/or oxygen vacancies [29, 30]. The emission peak at 562 nm (denoted by dotted line), only observed in the composite sample of TiO$_2$ calcined at 600 and 700 °C is assigned to the existence of localized energy levels in the forbidden energy gap. The existence of this peak is due to the presence of rutile phase which become responsible for the absorption red shift in TiO$_2$ as well the decrease in the recombination rate between the photogenerated electron and holes.

In PL analysis we noticed that increase in calcination temperature plays a significant role on PL characteristic features as well on its intensity. Increase in calcination temperature causes mainly the oxygen defect vacancies in TiO$_2$. The highest PL intensity was recorded for TiO$_2$ powder calcined at 400 °C, which may be due to the self-trapped excitons recombination generated due to the combined effect of oxygen vacancies and particle size. In contrast, the lowest PL intensity was noticed for bulk TiO$_2$ powder prepared at 600 and 700 °C; this occurs due to the increase in crystallinity and the composite nature of TiO$_2$ powder, which implies the appearance of rutile phase. The rutile phase becomes responsible for the decrease in peak intensity at 396, 411 and 418 nm and appearance of the peak at 559 nm in the visible region. These peaks were responsible for the UV emission, radiative defects, back transferring of electrons from CB to the VB as well decrease in the recombination of electron–hole pairs; therefore on the basis of PL analysis we believe that the composite powder will show enhanced photocatalytic activity for the selected pollutants.

3.6 Raman Analysis

Raman spectroscopy is one of the most effective characterization tools for the study of crystalline structure, phase transformation, crystallinity and defect structure associated with the materials. The change in Raman peaks position, line width and shape of the E$_g$ Raman mode are related to phonon confinement, shape and morphology distribution of various TiO$_2$ nanostructures, oxygen vacancies and to increase in temperature [22, 31]. Figure 7 illustrates the Raman spectra of TAF$_1$ sample powder calcined at 400–700 °C.

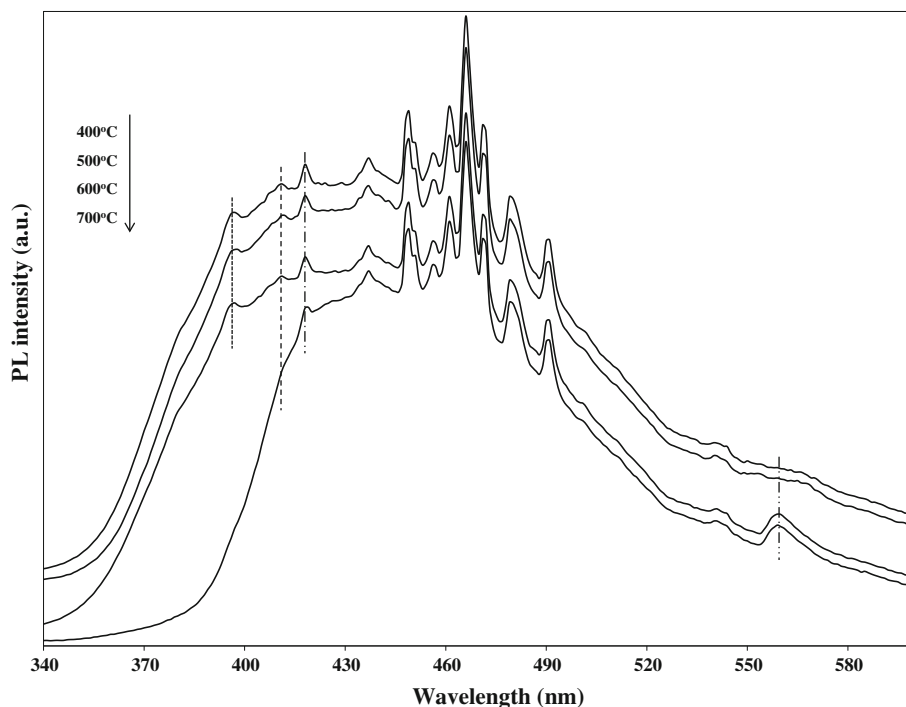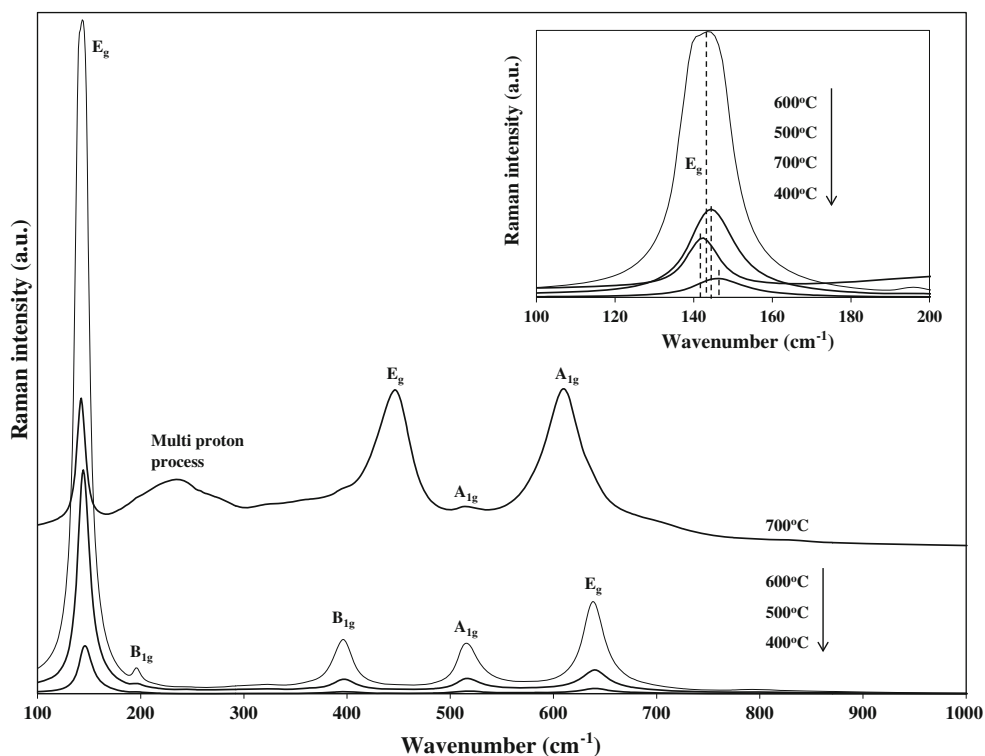**Fig. 6** PL spectra of TAF$_1$ powder calcined at different temperature

Fig. 7 Raman spectra of TAF$_1$ powder calcined at different temperature, (*inset*) Raman band (E$_g$) shift at different temperature

The anatase phase is characterized by the tetragonal space group of I41/amd and according to factor group analysis anatase has six Raman active modes ((1A$_{1g}$, 2B$_{1g}$ and 3E$_g$), while rutile structure is characterized by the tetragonal space group of P42/mnm and possess five Raman active modes (B$_{1g}$, multi-proton process, E$_g$, A$_{1g}$ and B$_{2g}$) [32]. In the present analysis, four Raman transitions at Eg (143 cm^{-1}), B$_{1g}$ (395 cm^{-1}), A$_{1g}$ (515 cm^{-1}) and E$_g$ (638 cm^{-1}) were observed for anatase TiO$_2$ calcined at 400 and 500 °C. The B$_{1g}$ mode at 195 cm^{-1} was observed for anatase TiO$_2$ calcined at 600 °C, the absence of this peak (B$_{1g}$—195 cm^{-1}) and the low Raman intensity

indicates that amorphous nature still remain in the powder calcined at 400 and 500 °C. All the bands assigned to anatase phase become sharp and strong after calcination at 600 °C, this is due to the increase in crystallinity in the sample. These results are in agreement with those of XRD. The variation in FWHM (full width at half maximum) in Raman bands are clearly visible, it has been observed that with increase in calcination temperature; $FWHM_{600} > FWHM_{500} > FWHM_{400}$, respectively.

The samples calcined at 700 °C contain rutile as the major phase with anatase as the minor one, it shows three Raman transition for rutile, multi-proton process (233 cm^{-1}), E_g (446 cm^{-1}) and A_{1g} (610 cm^{-1}) and two anatase active modes, E_g (142 cm^{-1}) and A_{1g} (513 cm^{-1}). This result clearly reveals that both anatase and rutile phase are well preserved after calcination at 700 °C, which is consistent with XRD patterns. Furthermore, it is noteworthy that the anatase strongest mode E_g (144 cm^{-1}) starts decreasing in intensity indicating the anatase phase starts to transform into rutile phase, in pure anatase the value of the ratio A_{1g}/E_g is different from that of anatase–rutile mixture (anatase-A_{1g}/E_g, rutile-A_{1g}/E_g). It is obvious that using Raman spectroscopy the percentage of specific exposed facets in anatase phase can be measured [32]. In the present analysis, the difference in the Raman mode ratios (A_{1g}/E_g) for pure anatase and anatase–rutile mixture confirms that the percentage of specific exposed facets of anatase is changing into rutile TiO$_2$ during the calcination, and that is why the strongest Raman mode (E_g—144 cm^{-1}) of anatase decreases in intensity and the Raman modes for rutile develop, illustrating that ART is taking place.

Figure 7 inset shows the Raman band shift and broadening in E_g mode (144 cm^{-1}) of TiO$_2$ nanoparticles calcined at 400–700 °C. It is well confirmed that crystallite size in the nano range may affect the broadening and frequency shifting of the Raman peaks due to phonon confinement effect [31]. The present Raman band broadening and frequency shifting is not due to phonon confinement because according to XRD results the particle size increases dramatically with increase in calcination temperature. The anomalous variation in the intensities of the Raman bands, shifting towards lower wavenumber and broadening as a function of temperature may not be attributed to the increase in crystallite size only but may be because of crystallinity, existence of mixed phases (anatase-brookite and or anatase–rutile) and oxygen vacancies. TEM micrographs show the particles morphology versus increase in calcination temperature (see Fig. 5). The particles calcined at 600 °C are more compact and agglomerated and have high crystallinity in comparison with particles calcined at 500 and 400 °C. Such behaviour may also contribute towards Raman mode broadening and frequency shifting. The deviation from phonon confinement model observed in this study is attributed to crystallinity, composite nature of the samples and more specifically to the oxygen vacancy induced defects resulting into the change of O/Ti ratio (oxygen stoichiometry) for the TiO$_2$ particles calcined at various temperatures.

3.7 Photocatalytic Analysis

The photocatalytic activity of the prepared TFA$_1$ and TFA$_0$ powders and of Degussa P25 was studied by monitoring the degradation of MB dye solution, as shown in Fig. 8a. At low calcination temperature (400 °C) TFA$_1$ show higher catalytic activity than TFA$_0$, then at 500 °C both of the catalysts activity is approximately equal while at 600 and 700 °C again TFA$_1$ outperforms the TFA$_0$ in photocatalytic activity. This enhanced activity can be attributed to the composite nature of the powder, high crystallinity (see Sect. 3.1), surface defects, Ti^{+3} centers and oxygen vacancies (see Sect. 3.5). The synthesized samples follow the order of photocatalytic activity as: anatase–rutile (94:6) > Degussa P25 (anatase–rutile-amorphous content (71:27:2), specific surface area 50 m^2 g^{-1}, crystallite size of anatase (20.8 nm) and rutile (30.5 nm) [33]) > anatase-brookite (86:14) > anatase > anatase–rutile (7:93). The composite powders have shown higher activity than pure anatase due to a decrease in recombination rate, the intimate contact between TiO$_2$ composite phases may enhance the separation between photogenerated electrons and holes to be consumed in the occurring process redox reactions [34, 35]. There must be an optimum fraction of rutile phase in the composite mixture of anatase–rutile, in the present case it is 6 %, further increase in rutile fraction causes a decrease in photocatalytic activity. Due to the large particle size of the rutile phase, the specific surface area decreases; as a consequence the surface will have fewer active sites for the decomposition of MB. In addition to the decrease in surface area, rutile has lower degree of surface hydroxyl groups which are the main hole scavenger in the photocatalytic process. The concentration of absorbed hydroxyl group at the catalyst surface decreases as a consequence of rutile formation at high calcination temperature. In comparison to rutile, the conduction band in anatase has higher energy; thus electron transfer from the conduction band to the adsorbed oxygen (main electron scavenger) molecule is energetically easier at the anatase surface than rutile surface; moreover, due to the different crystal structure the adsorption capability of anatase for organic dye molecule is higher than rutile [36]. PL analysis depicts enhanced formation of oxygen vacancies, the photoinduced electrons bound to the oxygen vacancies could promote easy adsorption of O$_2$ molecules to the catalyst surface to generate superoxide radicals (O$_2^{\bullet-}$). The presence of oxygen vacancies in TiO$_2$ structure which are produced due to increase in calcination temperature are beneficial for
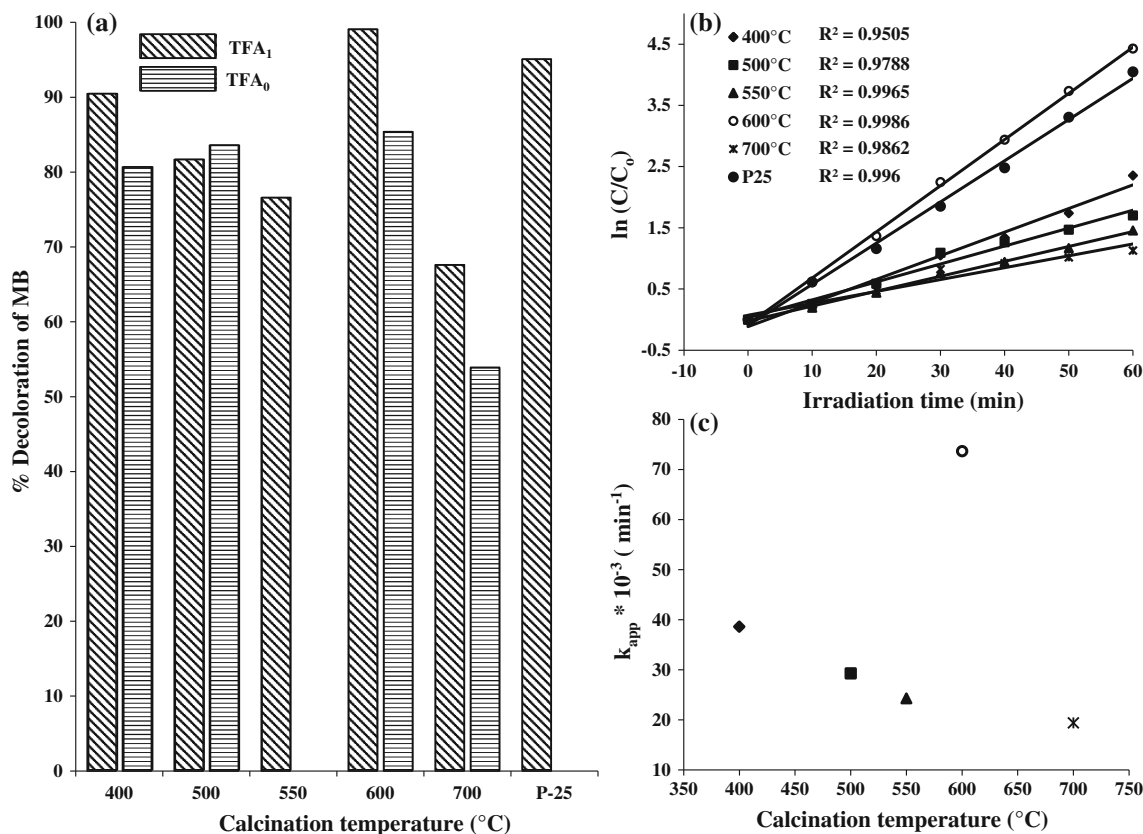
Fig. 8 a Photocatalytic decomposition of methylene blue by TFA_1 and TFA_0 catalyst powder calcined at different temperatures; **b** the plot of $-\ln(C/C_o)$ versus irradiation time for the TFA_1 powder calcined at different temperature and Degussa P25; **c** the plot of k_{app} against calcination temperature for the TFA_1 powders

photocatalytic reactions because O_2 is an active agent used in the oxidation of organic substances. Furthermore, absorption of electron by Ti^{+4} ions or oxygen vacancies on the surface of TiO_2 particles will give rise to Ti^{+3} centers, which are capable of trapping electron thus retards the recombination phenomena and improves photocatalytic activity.

Langmuir–Hinshelwood kinetics has been used to characterize the degradation of organic pollutants in TiO_2 photocatalysis [37, 38], which may be expressed as follows (Eq. (1)).

$$-\frac{dC}{dt} = k_{app}C_o \tag{1}$$

where, "dC/dt" represent the rate of change of in the organic pollutant concentration with respect to the illumination time "t", "k_{app}" is the apparent first order reaction rate constant and "C_o" the concentration of the organic pollutant.

Integration of the (Eq. 1) yield the following equation Eq. 2).

$$-\ln\left(\frac{C_o}{C}\right) = k_{app}t \tag{2}$$

The kinetics of the photocatalytic degradation of MB is illustrated in Fig. 8b. The plot between $\ln(C/C_o)$ versus irradiation time (t) gives a linear dependency with a correlation factor $R^2 > 0.95$ showing pseudo first order degradation kinetics for MB. Figure 8c demonstrates the variation of the rate constant (k_{app}) calculated for the decomposition of MB with TFA_1 powder calcined at different temperature, the powder calcined at temperature 600 °C gives highest value of k_{app} (0.074 min^{-1}) which is even higher than the commercially available Degussa P25 (0.067 min^{-1}).

To investigate further the activity of the catalyst powder with other pollutant, we tried MO and a mixture of MB and MO were used. Figure 9 illustrates the activity and the insert shows the first order kinetics of the TFA_1 and TFA_0 powders calcined at 600 °C and Degussa P25 for the decomposition of MO, while the insert demonstrates the first order kinetics of MO degradation. Similarly, the catalyst also showed enhanced activities for the decomposition of a mixture of MB and MO (see S6 in Supplementary Information), it was observed that the rate of decomposition of MO is delayed in comparison to MB. This may be due to its molecular structure

Fig. 9 Photocatalytic activity of catalyst samples TFA$_1$ and TFA$_0$ calcined at 600 °C and Degussa P25 for degradation of methyl orange, (*inset*) plot of ln(C/C$_o$) versus time
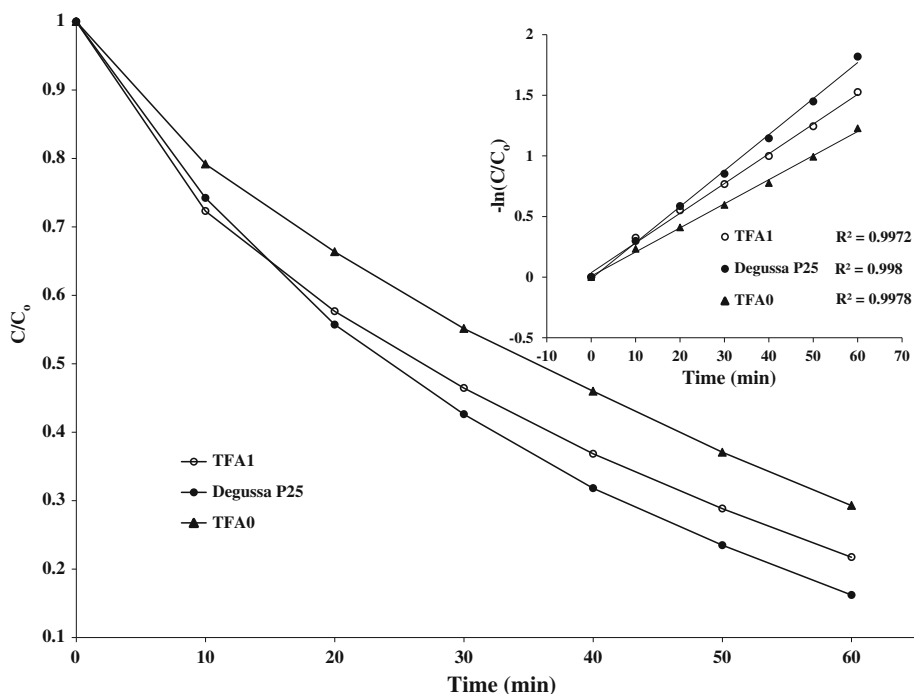
or the resistant nature of the intermediates formed, the insert shows the UV–Vis spectrum of mixture of MO and methylene blue.

4 Conclusions

- Anatase-brookite mixture was obtained as a result of acid (formic acid) hydrolysis of titanium alkoxide while in the absence of acid pure anatase TiO$_2$ formation occurs at 400 °C.
- Rutile fraction in the final material increases with increase in the water content in the hydrolysis step. This happens, because the acidity of the sol as well the chelating effect of the formate group decreases as a result a weakened gel network formation takes place, consequently a decrease in ART temperature occurs.
- FTIR study showed that formic acid chelates with titanium precursor in the monodentate coordination mode, while under the effect of increase in titanium butoxide content, the formate group forms bidentate bridging linkage with titanium atoms.
- The effect of the structural transformation from anatase to composite mixture of anatase–rutile has been observed in the PL intensity as well in the Raman spectra. Raman band broadening and shifting was observed with increase in calcination temperature due to increase in crystallinity, composite nature of the powder and oxygen vacancy induced defects.

- Photocatalytic studies showed that the formic acid modified sample, TFA$_1$ (calcined at 600 °C) with an anatase/rutile mixture of 94:6 was more effective than Degussa P25, TFA$_1$ (calcined at 400 °C) with anatase/brookite mixture of 86:14, TFA$_1$ (calcined at 550 °C) with pure anatase and TFA$_1$ (calcined at 700 °C) with anatase/rutile mixture of 7:93 for the degradation of MB, showing that composite mixture is more effective than either phase alone. In addition, Ti^{+3} centers, oxygen vacancies and increase in the degree of crystallinity due to increase in temperature may also contribute towards enhanced activity although there is drastic increase in crystallite size. The photocatalytic decompositions of MO and a mixture of MB and MO were also investigated with TFA$_1$ and TFA$_0$ catalyst powders and compared with Degussa P25. It was observed that MO showed decreased degradation compared to MB, this may be due the resistant nature of its molecular structure or the intermediate products formed in the photocatalytic process.

References

1. Ying L, Hon LS, White T, Withers R, Hai LB (2003) Mater Trans 44:1328

2. Sahni S, Reddy SB, Murty BS (2007) Mater Sci Eng, A 452–453:758
3. Xu N, Shi Z, Fan Y, Dong J, Shi J, Hu MZC (1999) J Ind Eng Chem Res 38:373
4. Mao L, Li Q, Dang H, Zhang Z (2005) Mater Res Bull 40:201
5. Zhu J, Zhang J, Chen F, Iino K, Anpo M (2005) Top Catal 35:261
6. Zhang D, Qi L, Ma J, Cheng H (2002) J Mater Chem 12:3677
7. Schaefer DW, Martin JE, Wiltzius P, Cannell DS (1984) Aggregation of colloidal silica. In: Family F, Landau DP (eds) Kinetics of aggregation and gelation. Elsevier, Amsterdam
8. Yu Y, Xu D (2007) J Appl Catal B Environ 73:166
9. Nguyen TV, Choi DJ, Yang OB (2005) Res Chem Intermed 31:483
10. Suresh C, Biju V, Mukundan P, Warrier KGK (1998) Polyhedron 17:3131
11. Yin H, Wada Y, Kitamura T, Kambe S, Murasawa S, Mori H, Sakata T, Yanagida S (2001) J Mater Chem 11:1694
12. Zhang H, Banfield JF (2000) J Phys Chem B 104:3481
13. Chen Z, Zhao G, Li H, Han G, Song B (2009) J Am Ceram Soc 92:1024
14. Liu Y, Wang Z, Wang W, Huang W (2014) J. Cataly 310:16
15. Bischoff BL, Anderson MA (1995) Chem Mater 7:1772
16. Zelenak V, Vargova Z, Gyoryova K (2007) Spectrochim Acta Mol Biomol Spectros 66:262
17. Nakamoto K (1997) Infrared and Raman spectra of inorganic and coordinated compounds, part b: application in coordination, organometallic and bioinorganic chemistry. John Wiley and Sons Inc., Hoboken
18. Nolan NT, Seery MK, Pillai SC (2009) J Phys Chem C 113:16151
19. Coronado DR, Gattorno GR, Pesqueira MEE, Cab C, Coss R, Oskam G (2008) Nanotechnology 19:145605
20. Valencia S, Marin JM, Restrepo G (2010) Open Mater Sci J 4:9
21. Deng H, Hossenlopp JM (2004) J Phys Chem B 109:66
22. Mathpal MC, Tripathi AK, Singh MK, Gairola SP, Pandey SN, Agarwal A (2013) Chem Phys Lett 555:182
23. Serpone N, Lawless D, Khairutdinov R (1995) J Phys Chem 99:16646
24. Bouras P, Stathatos E, Lianos P (2007) Appl Catal B Environ 73:51
25. Wang Y, Zhang S, Wu X (2004) Nanotechnology 15:1162
26. Choudhury B, Dey M, Choudhury A (2013) Shallow and deep trap emission and luminescence quenching of TiO_2 nanoparticles on Cu doping. Appl Nanosci. doi:10.1007/s13204-013-0226-9
27. Li D, Haneda H, Hishita S, Ohashi N, Labhsetwar N (2005) J Fluorine Chem 126:69
28. Khan H, Berk D (2013) J Sol-Gel Sci Technol 68:1
29. Xu J, Shi S, Li L, Zhang X, Wang Y, Chen X, Wang J, Lv L, Zhang F, Zhong W (2010) J Appl Phys 107:053910
30. Zhou J, Takeuchi M, Ray AK, Anpo M, Zhao XS (2007) J Colloid Interface Sci 311:497
31. Choi HC, Jung YC, Kim SB (2005) Vib Spectr 37:33
32. Yan J, Wu G, Guan N, Li L, Li Z, Cao X (2013) Phys Chem Chem Phys 15:10978
33. Jensen H, Pedersen JH, Jorgensen JE, Pedersen JS, Joensen KD, Iversen SB, Sogaard EG (2006) J Exp Nanosci 1:355
34. Yu J, Yu H, Cheng B, Zhou M, Zhao X (2006) J Mol Catal A: Chem 253:112
35. Ardizzone S, Bianchi CL, Cappelletti G, Gialanella S, Pirola C, Ragaini V (2007) J Phys Chem C 111:13222
36. Chen DC, Wang Z, Liao ZF, Maic YL, Zhang MQ (2007) Polym Test 26:202
37. Asenjo NG, Santamaria R, Blanco C, Granda M, Alvarez P, Menendez R (2013) Carbon 55:62
38. Qourzal S, Barka N, Tamimi T, Assabbane A, Ichou YA (2008) Appl Catal A Gen 334:386